Beam

The Race to Make the Laser

Jeff Hecht

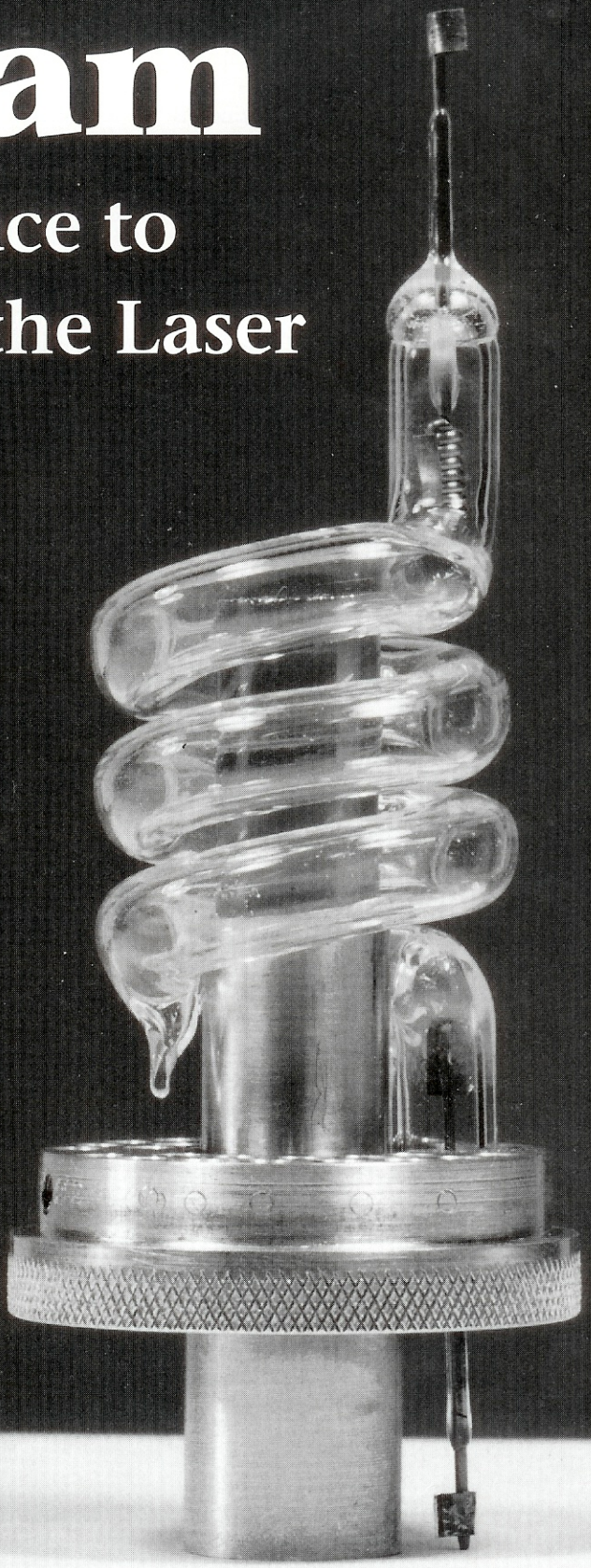

Forty-five years ago this year, physicist Theodore Maiman and his colleagues succeeded in making the first laser work at Hughes Research Laboratories in Malibu, Calif. Maiman performed the experiment on May 16, 1960, using an elegant ruby rod placed in a spring-shaded flash lamp. This article is adapted from Jeff Hecht's new book describing the science, politics and passion surrounding the great laser race; *Beam: The Race to Make the Laser* was published in March 2005 by Oxford University Press.

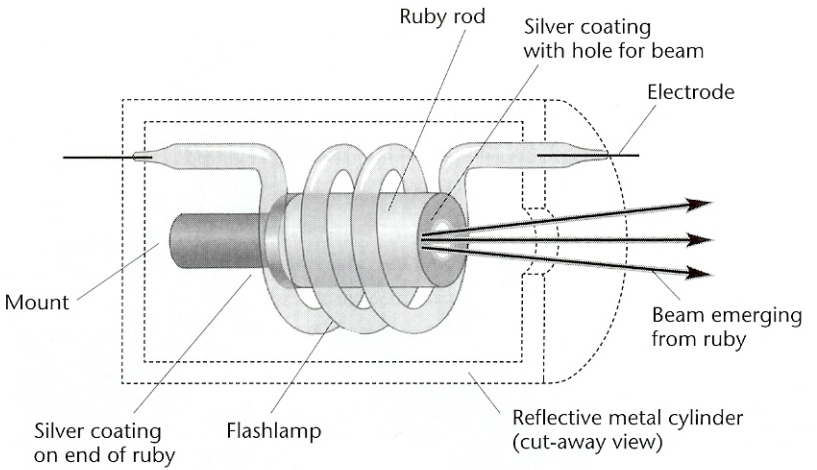

Structure of Maiman's first laser.

BEAM: THE RACE TO MAKE THE LASER

Hughes Research Laboratory, courtesy AIP Emilio Segrè Visual Archives

Theodore Maiman and Irnee D'Haenens display the first laser a quarter century after they made it.

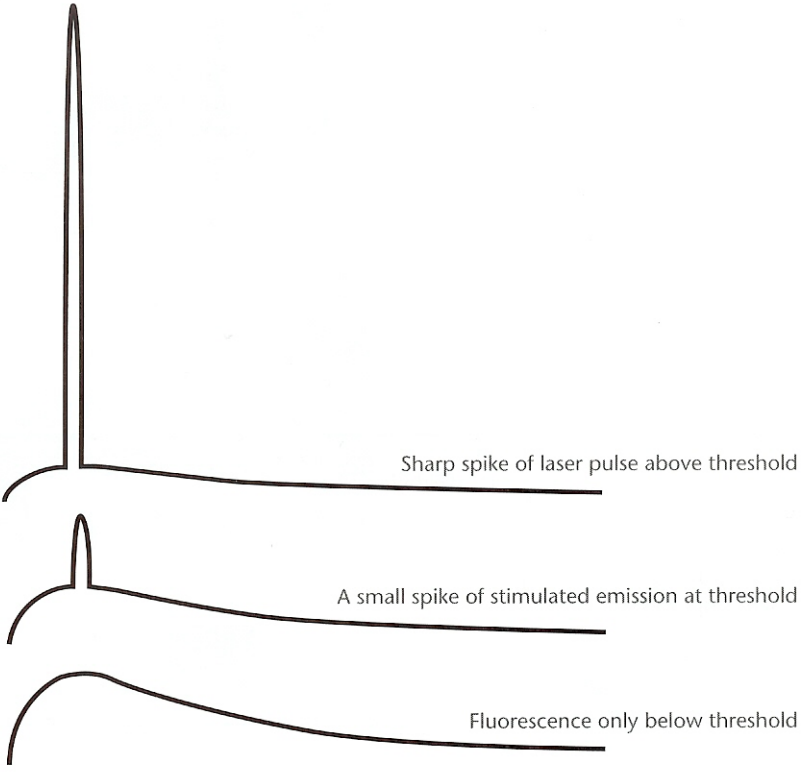

Ruby laser pulses rise and fall much faster than fluorescence produced by lower-power illumination. When Maiman started with modest flashlamp pulses, he saw only the rise and slow fluorescence (*bottom*). At laser threshold, a small spike of stimulated emission (*center*). When the flashlamp power exceeded the laser threshold, stimulated emission extracted energy from the ruby in a brief burst much shorter and more intense than the fluorescence he saw at lower flashlamp powers (*top*).

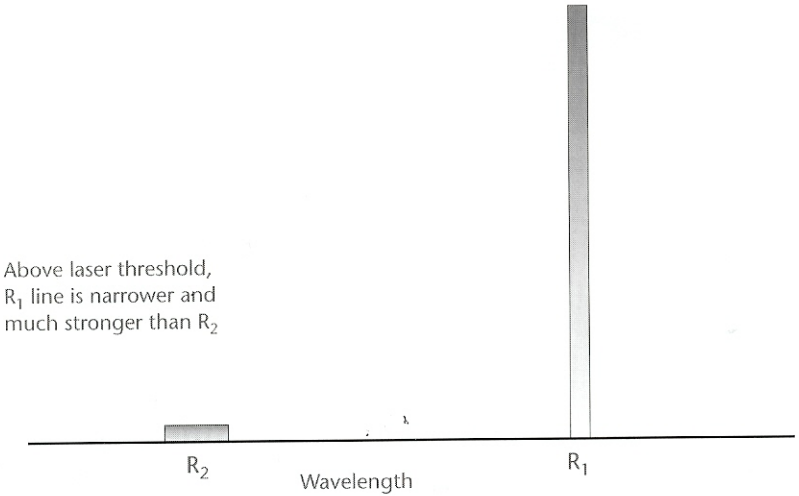

Laser operation narrowed the range of wavelengths and shifted the balance between the two red lines of ruby. Spontaneous emission from ruby (*bottom*) was fairly evenly divided between two lines called R_1 and R_2. Above laser threshold, laser oscillation narrowed the R_1 line and greatly increased its power, leaving the R_2 line weak (*top*). Maiman had predicted this effect, and he considered observing it proof of laser operation.

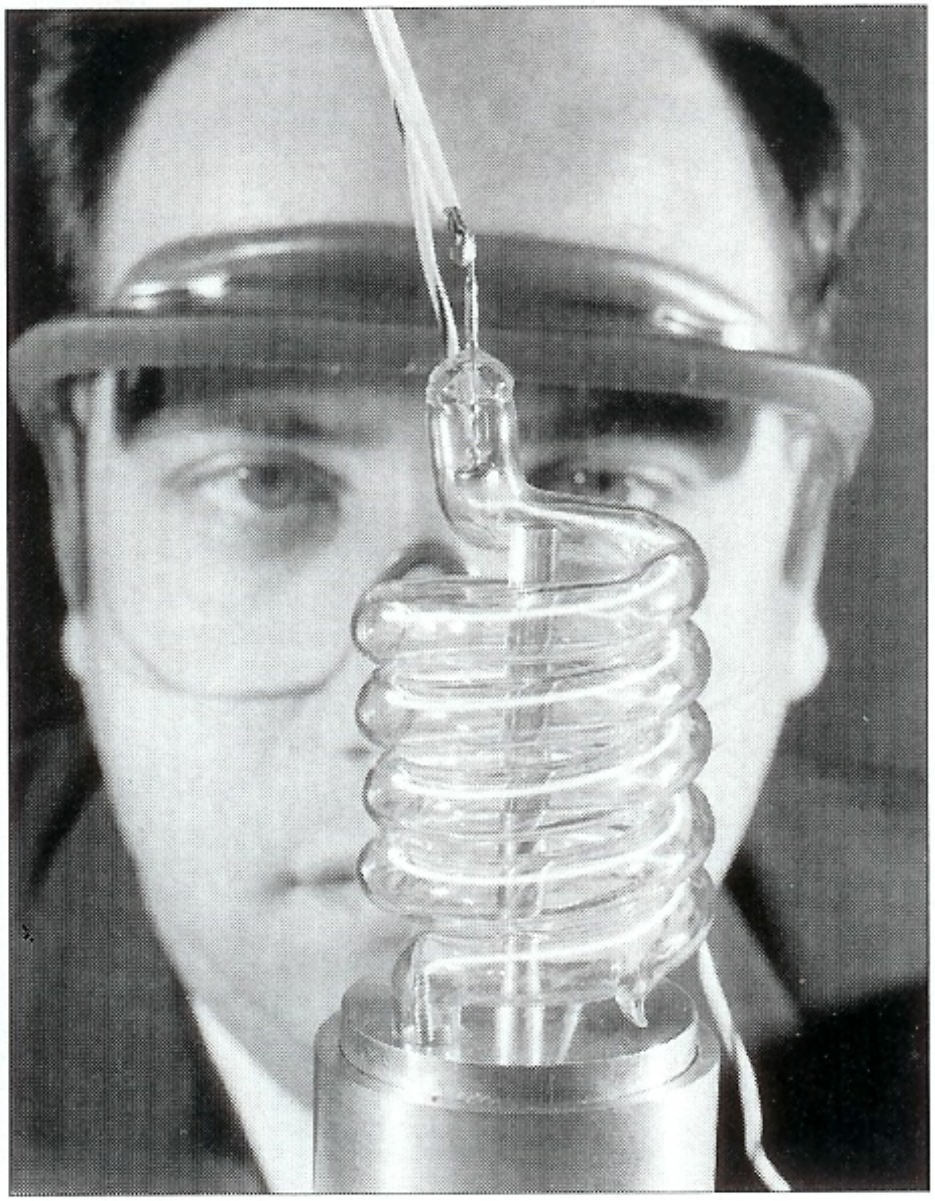

"The output trace started to shoot up in peak intensity and the initial decay time rapidly decreased," Maiman wrote. "Voilà. This was it! The laser was born!"

When it came time to announce Maiman's laser, Hughes's public relations firm hired a top photographer to take pictures. The photographer liked to get shots of people behind their inventions, but Maiman's first laser was too small, so he insisted on using a larger flashlamp and ruby rod. This photo was widely published as the "first" laser, and when other researchers tried to duplicate Maiman's work, they used this larger flashlamp to pump their ruby rods. Although they had the wrong lamp, their experiments worked within a few weeks.

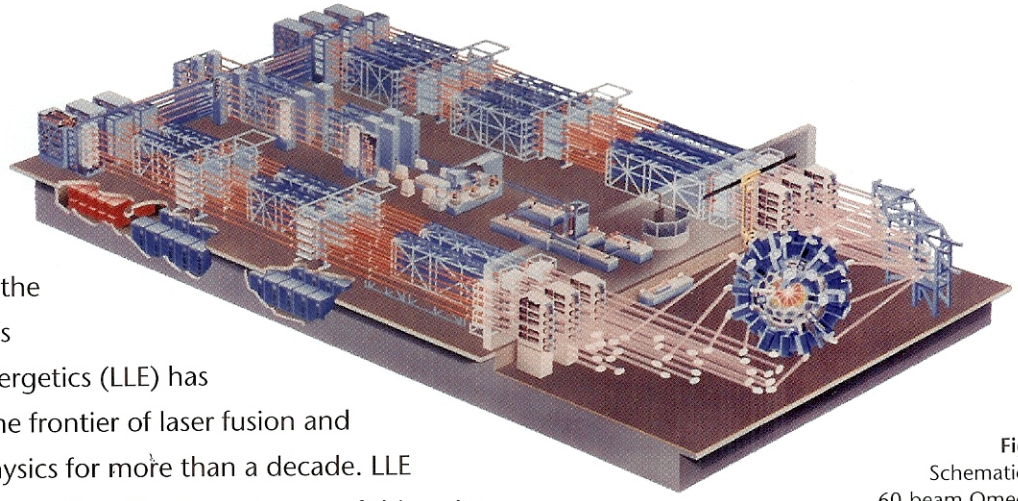

The 60-beam Omega laser system at the University of Rochester's Laboratory for Laser Energetics (LLE) has been a workhorse on the frontier of laser fusion and high-energy-density physics for more than a decade. LLE scientists are currently extending the performance of this unique, direct-drive laser system by adding high-energy petawatt capabilities.

Figure 1.
Schematic of the 60-beam Omega laser system showing the beam-lines and target chamber.

	Short-Pulse Capability	Long-Pulse Capability
Number of beamlines	2	4
Maximum on-target energy	2.6 kJ	6.5 kJ
On-target wavelength	1,053 nm	351 nm
Pulse-width range	1 to 100 ps	0.1 to 10 ns
Focal-spot diameter	20 to 1,000 μm	100 to 5,000 μm

Table 1: Omega EP Performance Goals
For short pulses, the on-target energies are limited by the demonstrated 10-ps grating-damage threshold of 4.3 J/cm^2. For long pulses, the on-target energies are limited by the anticipated 1-ns UV high-reflectivity coating damage threshold of 7 J/cm^2.

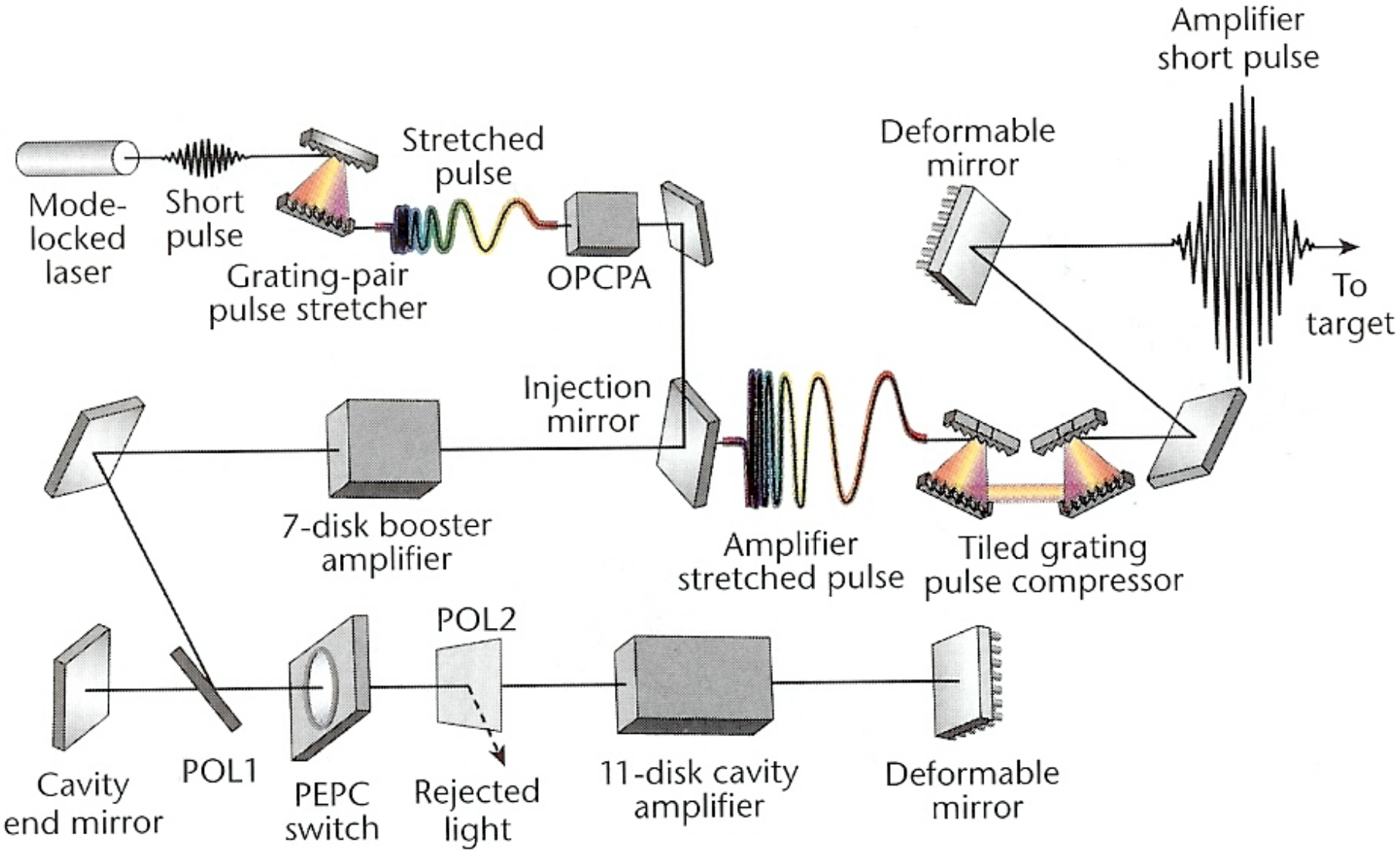

Figure 3. Schematic of an Omega EP petawatt beamline highlighting the enabling technologies to meet the performance objectives. These technologies include OPCPA, large-aperture laser amplifiers, a plasma-electrode Pockels cell switch, deformable mirrors and high-damage-threshold tiled gratings.

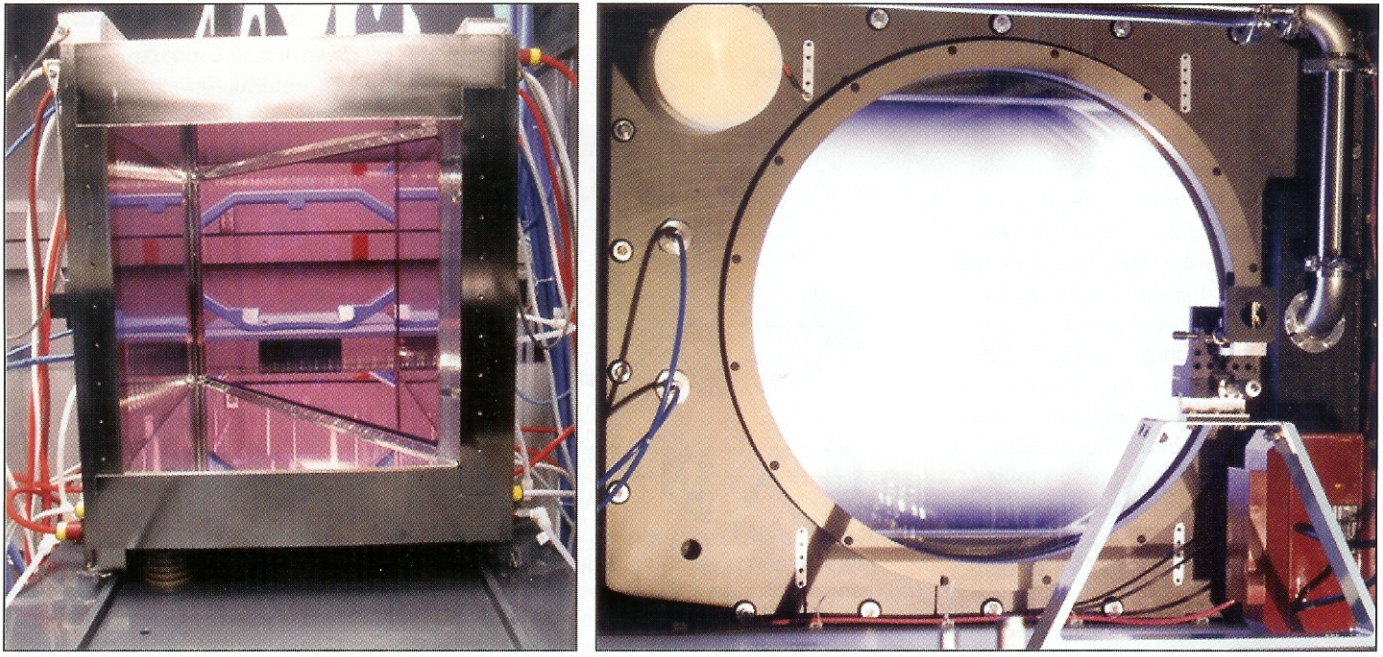

(a) (b)

Figure 4. (a) LLE-designed and built single-segment amplifier module with a 40-cm clear aperture. These modules are stacked end-to-end to form an 11-disk main amplifier and a 7-disk booster amplifier in each beamline. (b) Test firing of LLE-designed and built PEPC. The LLE PEPC has a contrast ratio that exceeds 1,000:1, providing increased protection from potentially damaging target retroreflections.

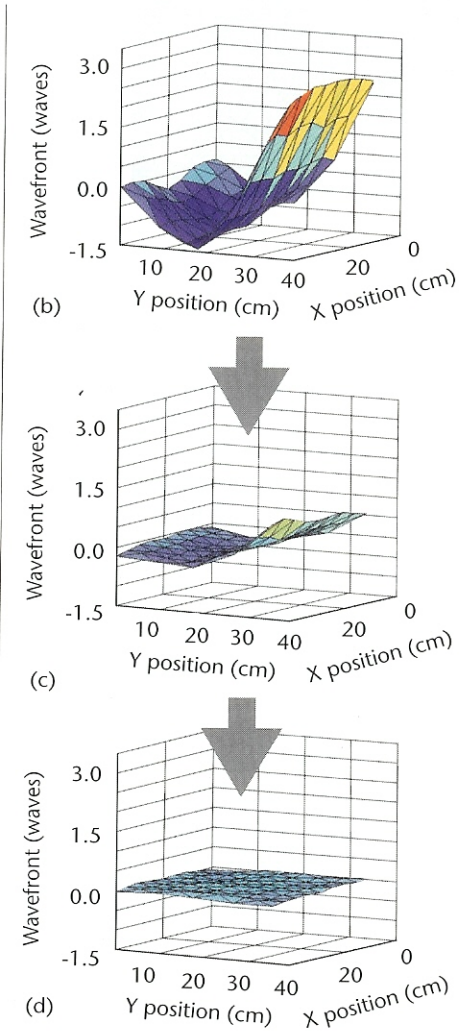

Figure 5. (a) Photograph showing the LLE assembly of a large-aperture deformable mirror. Three reflected wavefront measurements were performed during closed-loop tests of the wavefront control system. (b) The pre-correction wavefront. (c-d) Flattening of the wavefront achieved using the closed-loop control system.

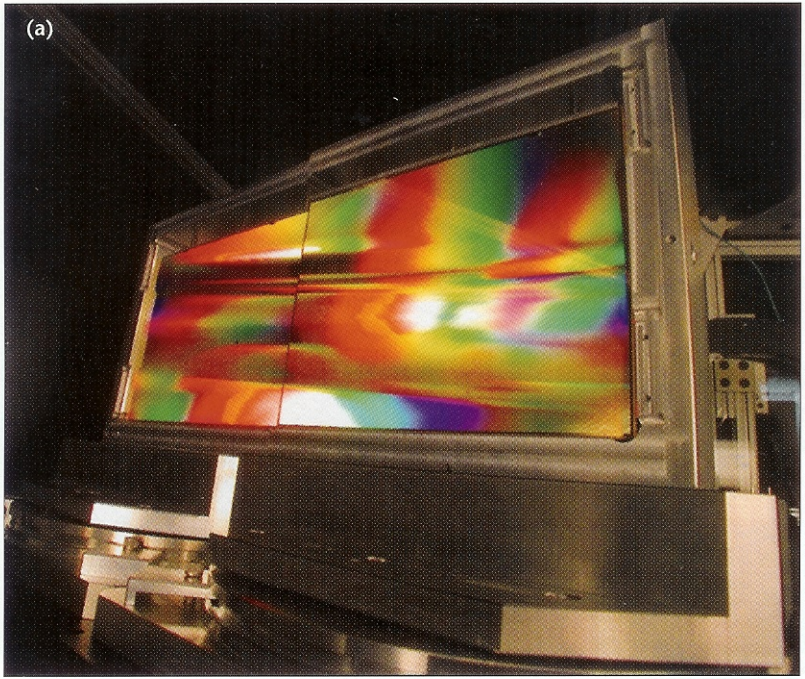

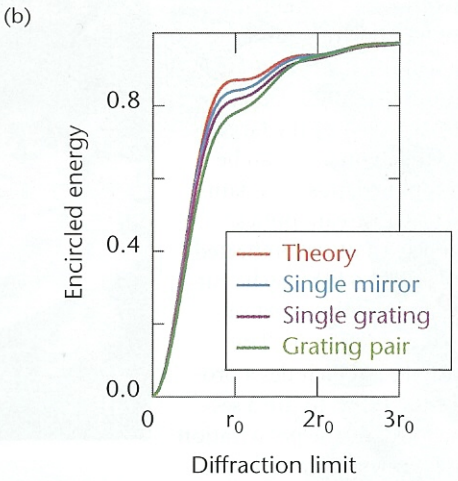

Figure 6. (a) Photograph of the initial tiled-grating setup used to demonstrate the concept's feasibility. (b) The encircled energy of the diffracted focal spot from the tiled-grating pair [shown in (a)] compared with that of a diffraction-limited focal spot.

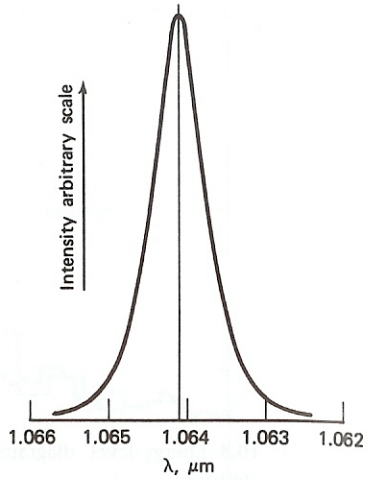

FIGURE 10.9 Spontaneous-emission spectrum of Nd^{3+} in YAG near the laser transition at $\lambda = 1.064$ μm. *Source:* Reference 7.

average ratio of laser frequency to the pump frequency is 0.5, and that the lamp efficiency (optical output/electrical input) is 0.5, we obtain

$$\mathscr{E}_{\text{lamp}} = \frac{N_{2t} h\nu_{\text{laser}}}{5 \times 10^{-2} \times 5 \times 10^{-2} \times 0.5 \times 0.5} \simeq 0.31 \text{ J/cm}^3$$

for the energy input to the lamp at threshold.

It is interesting to compare this last number to the figure of 300 J/cm^2 of surface area obtained in the ruby example of Section 10.2. For reasonable dimension crystals (e.g., length = 5 cm, r = 2 mm), we obtain $\mathscr{E}_{\text{lamp}} = 0.2$ J. We expect the ruby threshold to exceed that of Nd^{3+} : YAG by three orders of magnitude, which is indeed the case.

(b) *Continuous Operation.* The minimum power needed to maintain N_{2t} atoms (per unit volume) in level 2 is just prior to attaining threshold

$$P_{\text{min}} = \frac{N_{2t} h\nu}{t_2}$$

which for $t_2 \approx t_{\text{spont}}$, as is the case here, gives

$$P_{\text{min}} \approx \frac{N_t h\nu}{t_{\text{spont}}} \simeq 0.35 \text{ W/cm}^3$$

Taking the crystal diameter as 0.25 cm and its length as 3 cm and using the same efficiency factors assumed in the first part of this example, we can estimate the power input to the lamp at threshold as

$$P_{(\text{to lamp})} = \frac{0.35 \times (\pi/4) \times (0.25)^2 \times 3}{5 \times 10^{-2} \times 5 \times 10^{-2} \times 0.5 \times 0.5} \simeq 82 \text{ W}$$

which is in reasonable agreement with experimental values (Reference 6).

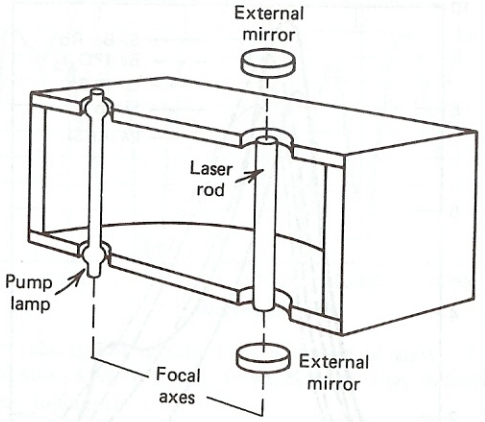

FIGURE 10.10 Typical continuous solid-state laser setup employing an elliptic cylinder housing for concentrating lamplight onto laser.

A typical arrangement used in continuous solid-state lasers is shown in Figure 10.10. The highly polished elliptic cylinder is used to concentrate the light from the lamp, which is placed along one focal axis, onto the laser rod, which occupies the other axis. This configuration guarantees that most of the light emitted by the lamp passes through the laser rod. The reflecting mirrors are placed outside the cylinder.

10.4 THE NEODYMIUM-GLASS LASER

One of the most useful laser systems is that which results when the Nd^{3+} ion is present as an impurity atom in glass (Reference 8).

The energy levels involved in the laser transition in a typical glass are shown in Figure 10.11. The laser emission wavelength is at $\lambda = 1.059$ μm,

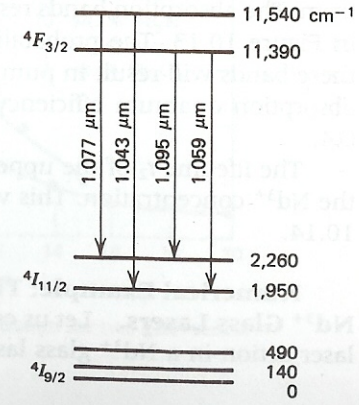

FIGURE 10.11 Energy-level diagram for the ground state and the states involved in laser emission near 1.059 μm for Nd^{3+} in a rubidium potassium barium silicate glass. *Source:* Reference 8.

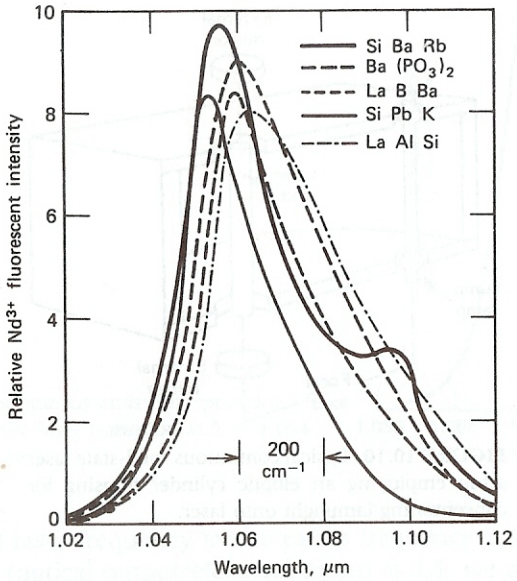

FIGURE 10.12 Fluorescent emission of the 1.06 μm line of Nd^{3+} at 300°K in various glass bases. *Source:* Reference 8.

and the lower level is approximately 1950 cm^{-1} above the ground state. As in the case of Nd^{3+} : YAG described in Section 10.3, we have here a four-level laser since the thermal population of the lower laser level is negligible. The fluorescent emission near $\lambda = 1.06$ μm is shown in Figure 10.12. The fluorescent linewidth can be measured off directly and ranges, for the glasses shown, around 300 cm^{-1}. This width is approximately a factor of 50 larger than that of Nd^{3+} in YAG. This is due to the amorphous structure of glass, which causes different Nd^{3+} ions to "see" slightly different surroundings. This makes their energy splittings vary slightly. Different ions consequently radiate at slightly different frequencies, causing a broadening of the spontaneous emission spectrum. The absorption bands responsible for pumping the laser level are shown in Figure 10.13. The probability that the absorption of a photon in any of these bands will result in pumping an atom to the upper laser level (i.e., the absorption quantum efficiency) has been estimated (Reference 8) at about 0.4.

The lifetime t_2 of the upper laser level depends on the host glass and on the Nd^{3+} concentration. This variation in two glass series is shown in Figure 10.14.

Numerical Example: Threshold for CW and Pulsed Operation of Nd^{3+} Glass Lasers. Let us estimate first the threshold for continuous (CW) laser action in a Nd^{3+} glass laser using the following data:

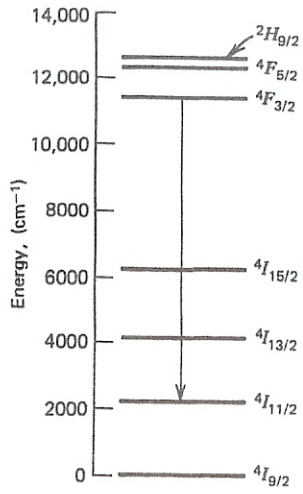

FIGURE 10.8 Energy-level diagram of Nd^{3+} in YAG. *Source:* Reference 6.

given inversion the optical gain constant γ in Nd^{3+} : YAG is approximately 75 times that of ruby. This causes the oscillation threshold to be very low and explains the easy continuous (CW) operation of this laser compared to ruby.

The absorption responsible for populating the upper level takes place in a number of bands between 13,000 and 25,000 cm^{-1}.

Numerical Example: Threshold of an Nd^{3+}:YAG Laser. (a) *Pulsed Threshold.* First, we estimate the energy needed to excite a typical Nd^{3+} : YAG laser on a pulse basis so that we can compare it with that of ruby. We use the following data:

$$l = 20 \text{ cm} \quad \text{(length optical resonator)}$$

$$L = 4\% \text{ (= loss per pass)}, \qquad t_c \simeq \frac{l}{Lc} = 1.6 \times 10^{-8} \text{ sec}$$

$$n = 1.5$$

$$\lambda = 1.064 \ \mu\text{m}$$

$$t_{\text{spont}} = 5.5 \times 10^{-4} \text{ sec}$$

$$\Delta\nu = 6 \text{ cm}^{-1}, \qquad \eta \simeq 1$$

Using the foregoing data in (9.1-16) gives

$$N_{2t} \simeq \Delta N_t = \frac{8\pi n^2 t_{\text{spont}} \Delta\nu}{\eta \, c t_c \lambda^2} \simeq 1.03 \times 10^{15} \text{ cm}^{-3}$$

Estimating that 5% of the exciting light energy falls within the useful absorp-

state. This time is much shorter than the 10^{-7} sec lifetime of the upper laser level $3S$. The condition $t_1 < t_2$ for population inversion in the $3S$-$2p$ transition (see Section 9.3) is thus fulfilled.

Another important point involves the level $1S$. Because of its long life, it tends to collect atoms reaching it by radiative decay from the lower laser level $2p$. Atoms in $1S$ collide with discharge electrons and are excited back into the lower laser level $2p$. This reduces the inversion. Atoms in the $1S$ states relax back to the ground state mostly in collisions with the wall of the discharge tube. For this reason, the gain in the 0.6328 μm transition is found to increase with decreasing tube diameter.

2. *1.15 μm Oscillation.* The upper laser level $2S$ is pumped by resonant (energy-conserving) collisions with the metastable 2^3S He level. It uses the same lower level as the 0.6328 μm transition and, consequently, also depends on wall collisions to depopulate the $1S$ Ne level.
3. *3.39 μm Oscillation.* This involves a $3S$-$3p$ transition and thus uses the same upper level as the 0.6328 μm oscillation. It is remarkable for the fact that it provides a small-signal[4] optical gain of about 50 dB/m. This large gain reflects partly the dependence of γ on λ^2 [see Eq. (8.4-4)] as well as the short lifetime of the $3p$ level, which allows the buildup of a large inversion.

Because of the high gain in this transition, oscillation would normally occur at 3.39 μm rather than at 0.6328 μm. The reason is that the threshold condition will be reached first at 3.39 μm and, once that happens, the gain "clamping" will prevent any further buildup of the population of $3S$. The 0.6328 μm laser overcomes this problem by introducing into the optical path elements, such as glass or quartz Brewster windows, that absorb strongly at 3.39 μm but not at 0.6328 μm. This raises the threshold pumping level for the 3.39 μm oscillation above that of the 0.6328 μm oscillation.

A typical gas-laser setup is illustrated by Figure 10.16. The gas envelope windows are tilted at Brewster's angle θ_B, so radiation with the electric field vector in the plane of the paper suffers no reflection losses at the windows. This causes the output radiation to be polarized in the sense shown, since the orthogonal polarization (the **E** vector out of the plane of the paper) undergoes reflection losses at the windows and, consequently, has a higher threshold.

10.6 THE CARBON DIOXIDE LASER

The lasers described so far in this chapter depend on electronic transitions between states in which the electronic orbitals (i.e., charge distributions around the atomic nucleus) are different. An example, consider the red (0.6328 μm) transition in Ne shown in Figure 10.15. It involves levels $2p^5 5s$ and $2p^5 3p$ so that in making a transition from the upper to the lower laser

[4] This is not the actual gain that exists inside the laser resonator, but the one-pass gain exercised by a very small input wave propagating through the discharge. In the laser, the gain per pass is reduced by saturation until it equals the loss per pass.

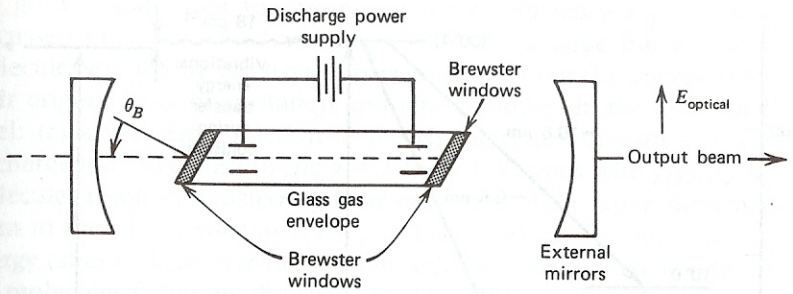

FIGURE 10.16 Typical gas laser.

level, one of the six outer electrons changes from a hydrogenlike state $5s$ (i.e., $n = 5$, $l = 0$) to one in which $n = 3$ and $l = 1$.

The CO_2 laser (Reference 12) is representative of the so-called molecular lasers in which the energy levels of concern involve the internal vibration of the molecules—that is, the relative motion of the constituent atoms. The atomic electrons remain in their lowest energetic states and their degree of excitation is not affected.

As an illustration, consider the simple case of the nitrogen molecule. The molecular vibration involves the relative motion of the two atoms with respect to each other. This vibration takes place at a characteristic frequency of $\nu_0 = 2326\ \text{cm}^{-1}$, which depends on the molecular mass as well as the elastic restoring force between the atoms (Reference 13). The quantum mechanical features of this system closely resemble those of the simple harmonic oscillator treated in Section 2.2. The degrees of vibrational excitation are discrete (i.e., quantized) and the energy of the molecule can take on the values $h\nu_0(v + \frac{1}{2})$, where $v = 0, 1, 2, 3, \ldots$. The energy-level diagram of N_2 (in its lowest electronic state) would then ideally consist of an equally spaced set of levels with a spacing of $h\nu_0$. The ground state ($v = 0$) and the first excited state ($v = 1$) are shown on the right side of Figure 10.17.

The CO_2 molecule presents a more complicated case. Since it consists of three atoms, it can execute three basic internal vibrations, the so-called normal modes of vibration. These are shown in Figure 10.18. In (*a*) the molecule is at rest. In (*b*) the atoms vibrate along the internuclear axis in a symmetric manner. In (*c*) the molecules vibrate symmetrically along an axis perpendicular to the internuclear axis—the bending mode. In (*d*) the atoms vibrate asymmetrically along the internuclear axis. This mode is referred to as the asymmetric stretching mode. In the first approximation, one can assume that the three normal modes are independent of each other, so the state of the CO_2 molecule can be described by a set of three integers (v_1, v_2, v_3) that correspond, respectively, to the degree of excitation of the three modes described. The total vibrational energy of the molecule is thus

$$E(v_1, v_2, v_3) = h\nu_1(v_1 + \tfrac{1}{2}) + h\nu_2(v_2 + \tfrac{1}{2}) + h\nu_3(v_3 + \tfrac{1}{2}) \qquad (10.6\text{-}1)$$

where N_1 and N_2 are the population densities of level 1 and 2, respectively. Using (8.5-2) and (8.5-3) in (8.5-5), we obtain

$$N_2[B_{21}\rho(\nu) + A] = N_1 B_{12}\rho(\nu)$$

and, substituting for $\rho(\nu)$ from (8.5-4),

$$N_2\left[B_{21}\frac{8\pi n^3 h\nu^3}{c^3(e^{h\nu/kT}-1)} + A\right] = N_1\left[B_{12}\frac{8\pi n^3 h\nu^3}{c^3(e^{h\nu/kT}-1)}\right] \tag{8.5-6}$$

Since the atoms are in thermal equilibrium, the ratio N_2/N_1 is given by the Boltzmann factor

$$\frac{N_2}{N_1} = \frac{g_2}{g_1}e^{-h\nu/kT} \tag{8.5-7}$$

Equating (N_2/N_1) as given by (8.5-6) to (8.5-7) gives

$$\frac{8n^3\pi h\nu^3}{c^3(e^{h\nu/kT}-1)} = \frac{A(g_2/g_1)}{B_{12}e^{h\nu/kT} - B_{21}(g_2/g_1)} \tag{8.5-8}$$

The last equality can be satisfied only when

$$B_{12} = B_{21}\frac{g_2}{g_1} \tag{8.5-9}$$

and, simultaneously,

$$\frac{A}{B_{21}} = \frac{8\pi n^3 h\nu^3}{c^3} \tag{8.5-10}$$

We can, using (8.5-10), rewrite the induced transition rate (8.5-1) as

$$(W'_{21})_i = \frac{Ac^3}{8\pi n^3 h\nu^3}\rho(\nu) = \frac{c^3}{8\pi n^3 h\nu^3 t_{\text{spont}}}\rho(\nu) \tag{8.5-11}$$

where $t_{\text{spont}} = 1/A$.

Equation (8.5-11) gives the transition rate per atom due to a field with a uniform (white) spectrum with energy density per unit frequency $\rho(\nu)$. In quantum electronics our main concern is in the transition rates that are induced by a monochromatic (i.e., single-frequency) field of frequency ν. Let us denote this transition rate as $(W_{21})_i$. We have established in Section 8.3 that the strength of interaction of a monochromatic field of frequency ν with an atomic transition is proportional to the lineshape function $g(\nu)$, so $(W_{21})_i \propto g(\nu)$. Furthermore, we would expect $(W_{21})_i$ to go over into $(W'_{21})_i$ as given by (8.5-11) if the spectral width of the radiation field is gradually increased from zero to a point at which it becomes large compared to the transition linewidth. These two requirements are satisfied if we take $(W_{21})_i$ as

$$(W_{21})_i = \frac{c^3\rho_\nu}{8\pi n^3 h\nu^3 t_{\text{spont}}}g(\nu) \tag{8.5-12}$$

where ρ_ν is the energy density of the electromagnetic field inducing the transitions. To show that $(W_{21})_i$ as given by (8.5-12) indeed goes over smoothly into (8.5-11) as the spectrum of the field broadens, we may consider the broad spectrum field as made up of a large number of closely spaced monochromatic components at ν_k with random phases and then by adding the individual transition rates obtained from (8.5-12) obtain

$$(W'_{21})_i = \sum_{\nu_k}(W_{21})_i(\nu_k) = \frac{c^3}{8\pi n^3 h t_{\text{spont}}}\sum_k \frac{\rho_{\nu_k}}{\nu_k^3}g(\nu_k) \tag{8.5-13}$$

where ρ_{ν_k} is the energy density of the field component oscillating at ν_k. We can replace the summation of (8.5-13) by an integral if we replace ρ_{ν_k} by $\rho(\nu)\,d\nu$ where $\rho(\nu)$ is the energy density per unit frequency; thus, (8.5-13) becomes

$$(W'_{21})_i = \frac{c^3}{8\pi n^3 h t_{\text{spont}}}\int_{-\infty}^{+\infty}\frac{\rho(\nu)g(\nu)\,d\nu}{\nu^3} \tag{8.5-14}$$

In situations where $\rho(\nu)$ is sufficiently broad compared with $g(\nu)$, and thus the variation of $\rho(\nu)/\nu^3$ over the region of interest [where $g(\nu)$ is appreciable] can be neglected, we can pull $\rho(\nu)/\nu^3$ outside the integral sign, obtaining

$$(W'_{21})_i = \frac{c^3}{8\pi n^3 h\nu^3 t_{\text{spont}}}\rho(\nu)$$

where we used the normalization condition

$$\int_{-\infty}^{\infty} g(\nu)\,d\nu = 1$$

This agrees with (8.5-11).

Returning to our central result, (8.5-12), we can rewrite it in terms of the intensity $I_\nu = c\rho_\nu/n$ (W/m^2) of the optical wave as

$$(W_{21})_i = \frac{Ac^2 I_\nu}{8\pi n^2 h\nu^3}g(\nu) = \frac{\lambda^2 I_\nu}{8\pi n^2 h\nu t_{\text{spont}}}g(\nu) \tag{8.5-15}$$

where c is the velocity of propagation of light in vacuum. This is the same result as that given by (8.3-9).

8.6 HOMOGENEOUS AND INHOMOGENEOUS BROADENING

The term broadening is used to denote the finite spectral width of the response of atomic systems to electromagnetic fields. The broadening may manifest itself, as an example, in a plot of the absorption as a function of frequency or in the frequency dependence of the gain of a laser medium. Such plots are included in Chapter 10.

We distinguish between two main classes of broadening mechanisms.

Homogeneous Broadening (Reference 6)

In this case, the atoms are indistinguishable and have the same transition energy $E_2 - E_1$. The broadening is due to one or a combination of the